Room-Temperature Perpendicular Exchange Coupling and Tunneling Anisotropic Magnetoresistance in an Antiferromagnet-Based Tunnel Junction

Y. Y. Wang, C. Song,* B. Cui, G. Y. Wang, F. Zeng, and F. Pan†

Laboratory of Advanced Materials, Department of Materials Science and Engineering, Tsinghua University, Beijing 100084, China

(Received 1 May 2012; published 27 September 2012)

We investigate the exchange coupling between perpendicular anisotropy (PMA) Co/Pt and IrMn in-plane antiferromagnets (AFMs), as well as tunneling anisotropic magnetoresistance (TAMR) in [Pt/Co]/IrMn/AlO_x/Pt tunnel junctions, where Co/Pt magnetization drives rotation of AFM moments with the formation of exchange-spring twisting. When coupled with a PMA ferromagnet, the AFM moments partially rotate with out-of-plane magnetic fields, in contrast with being pinned along the easy direction of IrMn for in-plane fields. Because of the superior thermal tolerance of perpendicular exchange coupling and the stability of moments in ~6 nm-thick IrMn, TAMR gets significantly enhanced up to room temperature. Their use would advance the process towards practical AFM spintronics.

DOI: 10.1103/PhysRevLett.109.137201 PACS numbers: 75.47.−m, 75.50.Ee, 75.70.Cn

The spin-valve effect stands out as a seminal phenomenon in the emerging field of spintronics for providing a fingerprint to determine giant magnetoresistance and spin injection [1,2]. Antiferromagnets (AFMs), which play a fundamental role in the spin-valve effect by establishing a reference magnetization direction, have been generally used as a static supporting material in spin-valve and magnetic tunnel junctions [3,4]. Despite the exchange bias (EB) discovered 50 years ago [5], the essential feature of ultrathin AFMs has been commonly ignored because they are overshadowed by their ferromagnetic counterparts [6]. Recently, Martí *et al.* [7] reported the behavior of antiferromagnetically ordered moments in IrMn exchange coupled to in-plane magnetized NiFe. In fact, perpendicular magnetic anisotropy (PMA) magnetic tunnel junctions are of great significance since they have a potential for realizing new-generation nonvolatile memory [8–10]; especially PMA is required for the reduction of critical current in spin-transfer torque switching [10]. Although the perpendicular EB with the focus of ferromagnets (FMs) has been discussed [11,12], a satisfying microscopic description and transport characteristics of AFMs when coupled with PMA FMs are still lacking.

A milestone observation for AFMs is the tunneling anisotropic magnetoresistance (TAMR) effect governed by the IrMn AFM [13], ascribed to the partial rotation of AFM moments in IrMn induced by in-plane magnetized NiFe, shedding promising light on AFM spintronics. Before that, the TAMR effect had been observed in FM-based systems, such as (Ga,Mn)As [14–16], Fe/GaAs/Au [17], Co_2MnSi/GaAs [18], and [Co/Pt]/AlO_x/Pt [19]. Unfortunately, almost all of these measurements were carried out below 100 K [14–19]; especially TAMR nearly disappeared above 100 K in NiFe/IrMn-based junctions with 1.5 and 3 nm IrMn [13], limiting their practical significance. The expected TAMR effect at room temperature (RT) in tunnel junctions, at the heart of its potential applicative interest, remains to be demonstrated. The experiments described here investigate the exchange coupling between PMA Co/Pt and the IrMn functional layer and confirm the RT TAMR effect in [Pt/Co]/IrMn-based junctions via electrical transport and magnetization reversal measurements.

The tunnel junctions Pt(5)/$[Co(0.5)/Pt(1)]_4$/Co(0.5)/IrMn(6)/AlO_x(2)/Pt(5) (units in nanometers) were grown by magnetron sputtering with an Ar pressure of 0.4 Pa on Si/SiO_2 wafers at RT. Co/Pt(111) multilayers allow manipulation of the moments within the IrMn active layer through exchange coupling. Magnetization studies were carried out using a vibrating sample magnetometer (VSM). The multilayers were then patterned into rectangle-shaped pillars of dimensions 5×3–$100 \times 60\ \mu m^2$, using photolithography and ion milling. The tunneling magnetoresistance was measured by a four-point contact geometry between 4–400 K with a bias of 100 μA. Here, we focus on data obtained from the $20 \times 12\ \mu m^2$ sample as they cover all the central features observed in the experiments.

To verify magnetic properties of full stack structures, we first show hysteresis loops in Fig. 1(a) measured with both vertical and parallel magnetic fields (H) at 300 K. The squared vertical hysteresis loop demonstrates a strong PMA of the multilayers with the coercive field (H_C) of 117 Oe. The presence of PMA profoundly affects the magnetoresistance probes [Figs. 1(b)–1(d)]. In Fig. 1(b), the resistance-area (RA) product of the junctions varying with vertical H is shown, referring to the easy axis of Co/Pt. Remarkably, the TAMR signal exhibits a hysteresis window with a stable high-resistance state (HRS) at initially applied positive H and a low-resistance state (LRS) at negative H, originating from the partial rotation of antiferromagnetic IrMn moments induced by Co/Pt magnetization, rather than Co/Pt itself [13,20], which will be discussed later in detail with the help of graphics in

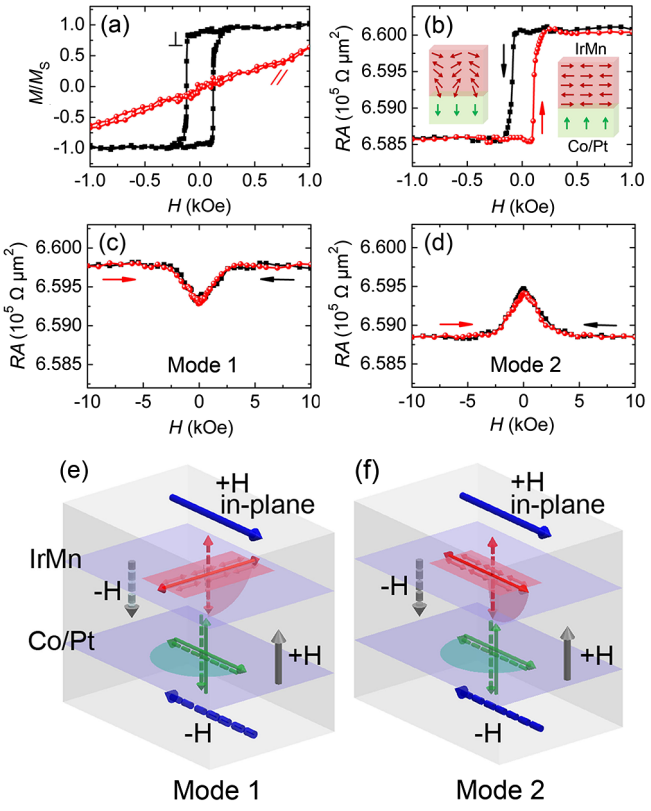

FIG. 1 (color online). (a) Magnetization loops of the stack structure with vertical H ($\perp$, squares) and parallel H (//, circles). Magnetoresistance acquired by sweeping H's which are (b) vertical to the films and (c),(d) parallel to the films, respectively. The sweep direction is given by arrows (first from $+H$ to $-H$). Insets of (b): schematic of no rotation (right) and exchange spring (left) of IrMn spins associated with Co/Pt magnetization. The only difference between (c) and (d) is that the in-plane H are orthogonal (mode 1) and parallel (mode 2) to the easy direction of IrMn, respectively, as sketched in (e) and (f). Arrows in the cubics represent the IrMn moments and the Co/Pt moments. All data were recorded at 300 K.

Figs. 1(e) and 1(f). Although the TAMR ratio is relatively small, ~0.236% [defined as (HRS–LRS)/LRS × 100%], the clearly detected signals illustrate the high sensitivity of transport properties in this system. Similar TAMR values were previously observed in FM-based junctions [17,19]. The results are surprisingly different when H's are applied in-plane. In Figs. 1(c) and 1(d), spin-valve-like signals of positive and negative TAMR are detected when the in-plane H are orthogonal and parallel to the easy direction of IrMn, defined as mode 1 and mode 2, respectively.

In general, EB systems exhibit an easy direction, e.g., unidirectional anisotropy [7,21], commonly defined by applying H during the growth [7,22] or postannealing [23,24]. In our case, the easy direction along the radius direction of the substrate holder is intimately correlated to the film growth procedure [25]. Figures 1(e) and 1(f) illustrate mode 1 and mode 2 for the same junction, where the only discrepancy between them is that the in-plane H are, respectively, orthogonal and parallel to the easy direction of IrMn, denoted by the solid arrows in the IrMn layer. Let us now discuss the high- or low-resistance variation with vertical fields. The Co/Pt moments are free to rotate in the reversed fields along their easy axes. Meanwhile, bulk IrMn moments are initially aligned in-plane due to their intrinsic character, producing a HRS because the Co/Pt and IrMn moments are orthogonal when vertical $+H$ are applied [right inset of Fig. 1(b)]. Afterwards, when fields sweep down to -1 kOe, an incomplete rotation of IrMn moments occurs (shadows in the IrMn layer), with the rotation angle of ~52° from the film plane (Fig. S4 of [25]). Ultimately, the IrMn spins align along $-H$ with a rotation of 90° at around -90 kOe. The parallel relationship between Co/Pt and IrMn leads to a LRS. This observed asymmetry between the two states (HRS/LRS) could be ascribed to the downward component of interfacial IrMn spins, which is an imprint of the domain pattern of as-deposited Co/Pt [26]. The initial tilt makes IrMn easier to rotate to a downward direction (Fig. S5 of [25]). Note that the domain-wall width (δ_W) in IrMn is calculated to be ~7.8 nm [25], indicating that the whole 6 nm IrMn layer is an exchange spring [left inset of Fig. 1(b)], and the rotation angle described above could be considered as the average of all the IrMn spins.

This situation changes dramatically with in-plane fields. The positive TAMR in mode 1 could be explained as follows: the Co/Pt moments (arrows in the Co/Pt layer) rotate with in-plane H (shadows in the Co/Pt layer), whereas the AFM moments in IrMn are persistently pinned along the easy direction [21] and the in-plane rotation could not occur. Obviously, the Co/Pt and IrMn moments are mutually orthogonal both at high positive and negative fields. At zero field, the Co/Pt moments are aligned parallel and antiparallel to the film normal at this demagnetized state, producing the resistance in the intermediate state between the HRS and the LRS (Fig. S6 of [25]). This case allows perpendicular → intermediate → perpendicular interactions between Co/Pt and IrMn with $+H \rightarrow$ zero-field $\rightarrow -H$, ensuring the positive TAMR. In mode 2, large in-plane $+H$ are applied along the easy direction of IrMn; corresponding to a parallel FM/AFM arrangement, a subsequent sweep of fields from $+H$ via zero field to $-H$ results in a parallel → intermediate → parallel change, accompanied by the negative TAMR.

In addition to the two specific positions, vertical and parallel, we plot in Fig. 2(a) the TAMR ratio as a function of out-of-plane rotation (θ) from $\theta = 90°$ to $\theta = 0°$. The TAMR ratio decreases gradually with rotation to in-plane, revealing that the IrMn moments are easier to reverse, showing larger TAMR signals with vertical H. Meanwhile, we have explored resistance variation with changing the angle from $\varphi = 90°$ (mode 1) to $\varphi = 0°$ (mode 2) with in-plane H of 5 kOe [Fig. 2(b)]. The RA product reaches its maximum when H's are orthogonal to

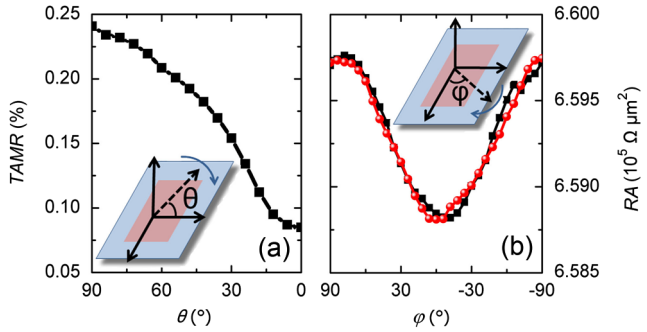

FIG. 2 (color online). (a) The TAMR values with the changing out-of-plane θ at 300 K. (b) In-plane angle φ dependent resistance with $H = 5$ kOe at 300 K. The insets are the sketches of measurement configurations.

the easy direction of IrMn ($\varphi = 90°$ and $-90°$), whereas the minimum is obtained in the parallel case ($\varphi = 0°$). Given that the Co/Pt moments rotate with H at all angles even in its hard axis, a perpendicular → parallel → perpendicular interaction of Co/Pt and IrMn moments induces an arc-shaped curve, confirming that the IrMn moments are fixed to the easy direction of AFMs with in-plane H.

The effects of rotating junction devices and stack films on the RA product and magnetization at representatively fixed H are shown in Fig. 3, which provides strong evidence for the TAMR effect based on AFMs [13]. The samples initially stay at a vertical field ($\theta = 90°$), then rotate to an in-plane field ($\theta = 0°$) and continue to rotate to $\theta = -90°$. Both the TAMR and VSM measurements were recorded by first applying $H = -5$ kOe, followed by setting $+H$ marked in each panel. During rotating the device in a 40 Oe field, a constant resistance is observed (top left panel in Fig. 3), indicating no exchange-spring action on the IrMn because of no significant rotation of the Co/Pt moments at this low field. However, the magnetization detected by VSM switches with the sample, with the magnetization from negativity to positivity (top right panel in Fig. 3). Note that the magnetization is sensitive to Co/Pt, whereas the tunneling transport is governed by IrMn. The field of 70 Oe begins to motivate the tilt of IrMn moments. At $H = 100$ Oe, clear TAMR is observed arising from a gradual rotation of the IrMn moments. When fields reach the H_C of 120 Oe, corresponding magnetization exhibits a butterfly curve, revealing higher magnetization obtained in vertical H. With further increasing H, the hysteresis windows in both panels decrease. While it increases to be saturated at 5 kOe, a nearly constant VSM signal is observed because Co/Pt is saturated at all angles. Differently, the resistance changes from a HRS to a LRS with θ rotating from 90° to −90° because of the exchange spring in IrMn. The intricate connection between the TAMR and VSM measurements offers an effective approach to prove that the magnetoresistance is indeed of AFM-based TAMR origin.

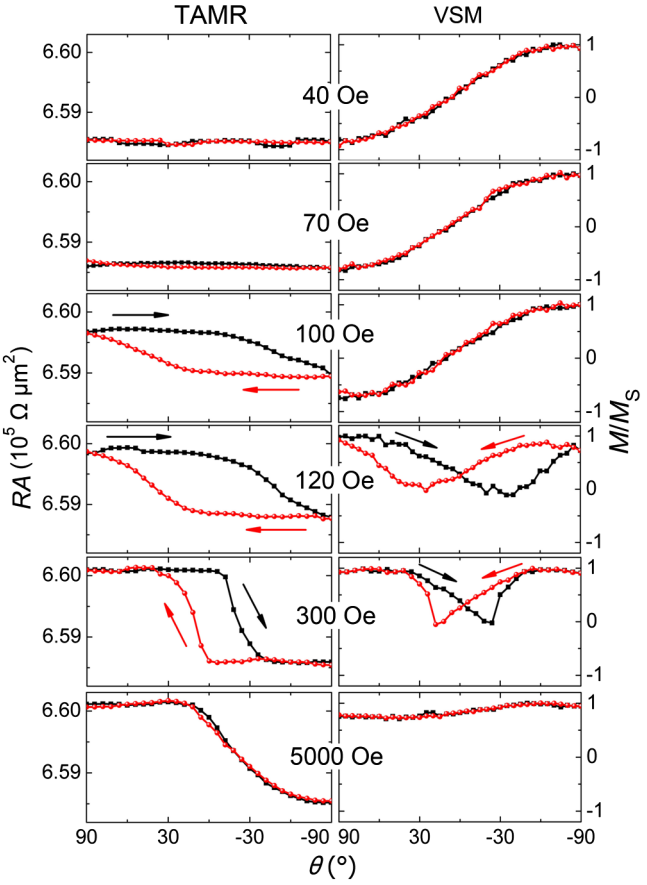

FIG. 3 (color online). The effects of rotating junctions and stack films on resistances (TAMR, left panels) and magnetization (VSM, right panels) in fixed fields at 300 K. The sample was rotated first from $\theta = 90°$ to $-90°$ (squares) and then backwards (circles).

We now turn towards the temperature dependent TAMR. Figures 4(a) and 4(b) illustrate the magnetoresistance curves with out-of-plane and in-plane H at 4 K, respectively. Compared to that at RT, the resistance trace with out-of-plane fields at 4 K exhibits the broadening of H_C and a resolvable bias field (H_E) [Fig. 4(a)], demonstrating the exchange coupling in [Pt/Co]/IrMn and the AFM-based TAMR effect. This is bolstered by the opposite horizontal shifts of magnetization loops at 4 K after the field-cooled procedure with ±10 kOe (Fig. S7 of [25]). The in-plane magnetoresistance trace in Fig. 4(b) shows the spin-valve-like behavior as that at RT. Temperature (T) dependent TAMR values are then presented in Fig. 4(c). Interestingly, the out-of-plane TAMR values keep almost constancy, ~0.236% (Fig. S8 of [25]), in contrast to a rapid decay of in-plane TAMR, from 0.171% to 0.070% as T increases from 4 to 300 K. These findings verify the superior thermal tolerance of perpendicular EB, which is crucial for the realization of TAMR at RT. In addition, the angular dependent RA product at $H = 5$ kOe at various temperatures is depicted in Fig. 4(d). For $\theta = 90°$–0°

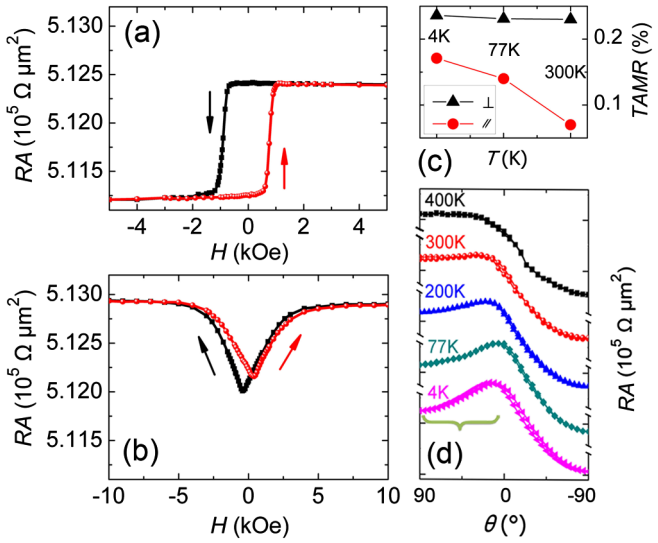

FIG. 4 (color online). Magnetoresistance acquired by (a) sweeping vertical and (b) parallel H at 4 K. (c) Temperature dependent TAMR ratio with vertical (⊥, triangles) and parallel (//, circles) fields. (d) The angular dependence of resistances at 5 kOe at five typical temperatures.

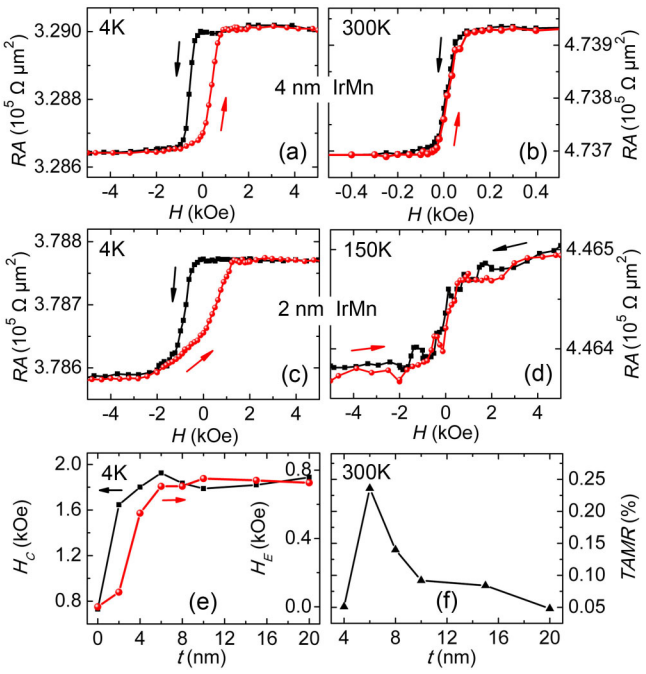

FIG. 5 (color online). Magnetoresistance of the 4 nm IrMn sample with H vertical to the films at (a) 4 K and (b) 300 K. The signals measured in the sample with the 2 nm IrMn at (c) 4 K and (d) 150 K. (e) t-dependent H_C and H_E at 4 K after a field-cooled procedure. (f) t-dependent TAMR ratio at 300 K.

(marked by a bracket), the slope of the curves decreases with enhancing T, producing a plateau at 400 K, reflecting the comparable resistances with vertical and parallel H. Because the resistance is manipulated by angles between Co/Pt and IrMn [25], a relatively larger resistance with parallel H ($\theta = 0°$) at 4 K reveals that the strong unidirectional anisotropy of IrMn stabilizes its moments along the easy direction. The anisotropy is reduced, and the partial rotation of IrMn becomes prevailing as T is enhanced, resulting in the higher resistance with vertical H. This verifies that the out-of-plane TAMR dominates at RT.

We now address the question whether RT TAMR exists with decreasing IrMn thickness (t). Figures 5(a)–5(d) exhibit magnetoresistance curves with vertical H at representative T for 4 and 2 nm IrMn samples. For 4 nm IrMn, typical TAMR curves are obtained at 4 K [Fig. 5(a)], which remains when $T = 300$ K [Fig. 5(b)], but with a decreasing magnitude from 0.116% to 0.051%. TAMR at 4 K is recognizable in Fig. 5(c) as $t = 2$ nm, whereas it vanishes just above 150 K [Fig. 5(d)], consistent with the TAMR signal up to 100 K in Ref. [13]. The squared TAMR curves for 6 nm IrMn [Fig. 1(b)], compared with an asymmetric hysteretic feature and reduced TAMR values for 2 nm IrMn, reveal that the AFM moments in thicker IrMn (~ 6 nm) are more stable (Fig. S9 of [25]), as a key to realizing RT TAMR.

The H_C and H_E for different t at 4 K after a field-cooled procedure are plotted in Fig. 5(e), showing the maximum at 6 nm [25], which is critical for building a stable exchange coupling [22,24,27–29]. For the samples with IrMn beyond 6 nm, e.g., 8, 10, 15, and 20 nm, we also observe TAMR signals [Fig. 5(f)]; however, as expected, this is less pronounced compared with the 6 nm IrMn sample (Fig. S10 of [25]). Hence, 6 nm could be an ideal AFM thickness for obtaining a combination of strong EB and TAMR. Particularly, the TAMR ratio drops rapidly between 6–10 nm [Fig. 5(f)], supporting the TAMR manipulated by the exchange spring with δ_W of $\sim$7.8 nm. The IrMn spins with the distance larger than this value cannot be triggered by Co/Pt, producing both exchange spring and bulk in the thick IrMn (Fig. S11 of [25]). The TAMR decays slower when $t = 10$–20 nm. This t-dependent tendency could be explained by spin flipping in IrMn: strong spin flipping occurs at the interface of exchange spring and bulk, but it becomes weaker in the bulk [30]. Therefore, the TAMR ratio dramatically drops when t increases just above δ_W, and then slowly decreases.

In summary, our Letter verifies that the antiferromagnetic moments in IrMn are persistently pinned along the easy direction of IrMn with in-plane fields due to the unidirectional anisotropy, whereas it is comparatively easy to achieve partial rotation associated with PMA Co/Pt with vertical fields. We demonstrate room-temperature TAMR in AFM-based tunnel junctions, which is due to two crucial aspects: superior thermal tolerance of perpendicular exchange coupling and stable antiferromagnetic moments in relatively thick IrMn (e.g., 6 nm). Practical applications of AFM spintronics are expected with a higher TAMR magnitude through optimizing the structure of the present junctions.

This work was supported by the National Natural Science Foundation of China (Grants No. 51202125 and No. 51231004) and the National Basic Research Program of China (Grant No. 2010CB832905).

*Corresponding author
songcheng@mail.tsinghua.edu.cn
†Corresponding author
panf@mail.tsinghua.edu.cn

[1] C. Chappert, A. Fert, and F. N. V. Dau, Nature Mater. **6**, 813 (2007).
[2] C. Song, M. Sperl, M. Utz, M. Ciorga, G. Woltersdorf, D. Schuh, D. Bougeard, C. H. Back, and D. Weiss, Phys. Rev. Lett. **107**, 056601 (2011).
[3] A. H. MacDonald and M. Tsoi, Phil. Trans. R. Soc. A **369**, 3098 (2011).
[4] P. Y. Yang, C. Song, F. Zeng, and F. Pan, Appl. Phys. Lett. **92**, 243113 (2008).
[5] W. H. Meiklejohn and C. P. Bean, Phys. Rev. **105**, 904 (1957).
[6] J. Sinova and I. Žutić, Nature Mater. **11**, 368 (2012).
[7] X. Martí *et al.*, Phys. Rev. Lett. **108**, 017201 (2012).
[8] S. Mangin, D. Ravelosona, J. A. Katine, M. J. Carey, B. D. Terris, and E. E. Fullerton, Nature Mater. **5**, 210 (2006).
[9] R. Sbiaa, R. Law, S. Y. H. Lua, E. L. Tan, T. Tahmasebi, C. C. Wang, and S. N. Piramanayagam, Appl. Phys. Lett. **99**, 092506 (2011).
[10] S. Ikeda, K. Miura, H. Yamamoto, K. Mizunuma, H. D. Gan, M. Endo, S. Kanai, J. Hayakawa, F. Matsukura, and H. Ohno, Nature Mater. **9**, 721 (2010).
[11] J. Sort, V. Baltz, F. Garcia, B. Rodmacq, and B. Dieny, Phys. Rev. B **71**, 054411 (2005).
[12] S. Maat, K. Takano, S. S. P. Parkin, and E. E. Fullerton, Phys. Rev. Lett. **87**, 087202 (2001).
[13] B. G. Park *et al.*, Nature Mater. **10**, 347 (2011).
[14] C. Gould, C. Rüster, T. Jungwirth, E. Girgis, G. M. Schott, R. Giraud, K. Brunner, G. Schmidt, and L. W. Molenkamp, Phys. Rev. Lett. **93**, 117203 (2004).
[15] C. Rüster, C. Gould, T. Jungwirth, J. Sinova, G. M. Schott, R. Giraud, K. Brunner, G. Schmidt, and L. W. Molenkamp, Phys. Rev. Lett. **94**, 027203 (2005).
[16] A. D. Giddings *et al.*, Phys. Rev. Lett. **94**, 127202 (2005).
[17] J. Moser, A. Matos-Abiague, D. Schuh, W. Wegscheider, J. Fabian, and D. Weiss, Phys. Rev. Lett. **99**, 056601 (2007).
[18] T. Uemura, M. Harada, K. Matsuda, and M. Yamamoto, Appl. Phys. Lett. **96**, 252106 (2010).
[19] B. G. Park, J. Wunderlich, D. A. Williams, S. J. Joo, K. Y. Jung, K. H. Shin, K. Olejník, A. B. Shick, and T. Jungwirth, Phys. Rev. Lett. **100**, 087204 (2008).
[20] A. Scholl, M. Liberati, E. Arenholz, H. Ohldag, and J. Stöhr, Phys. Rev. Lett. **92**, 247201 (2004).
[21] J. Nogués and I. K. Schuller, J. Magn. Magn. Mater. **192**, 203 (1999).
[22] R. Jungblut, R. Coehoorn, M. T. Johnson, J. aan de Stegge, and A. Reinders, J. Appl. Phys. **75**, 6659 (1994).
[23] L. Gao, X. Jiang, S. -H. Yang, J. D. Burton, E. Y. Tsymbal, and S. S. P. Parkin, Phys. Rev. Lett. **99**, 226602 (2007).
[24] J. Moritz, G. Vinai, and B. Dieny, IEEE Magn. Lett. **3**, 4000204 (2012).
[25] See Supplemental Material at http://link.aps.org/supplemental/10.1103/PhysRevLett.109.137201 for the details of in-plane magnetic field, temperature, and IrMn thickness dependent TAMR.
[26] S. van Dijken, M. Crofton, M. Czapkiewicz, M. Zoladz, and T. Stobiecki, J. Appl. Phys. **99**, 083901 (2006).
[27] G. Vallejo-Fernandez, L. E. Fernandez-Outon, and K. O'Grady, Appl. Phys. Lett. **91**, 212503 (2007).
[28] V. Baltz, J. Sort, S. Landis, B. Rodmacq, and B. Dieny, Phys. Rev. Lett. **94**, 117201 (2005).
[29] M. Ali, C. H. Marrows, and B. J. Hickey, Phys. Rev. B **67**, 172405 (2003).
[30] R. Acharyya, H. Y. T. Nguyen, W. P. Pratt, Jr., and J. Bass, J. Appl. Phys. **109**, 07C503 (2011).